Available online at www.sciencedirect.com

ScienceDirect

journal homepage: www.elsevier.com/locate/he

Preparation of methanation catalysts for high temperature SOEC by β-cyclodextrin-assisted impregnation of nano-CeO_2 with transition metal oxides

Patryk Błaszczak [a,*], *Adrian Mizera* [b], *Beata Bochentyn* [a], *Sea-Fue Wang* [c], *Piotr Jasiński* [d]

[a] *Faculty of Applied Physics and Mathematics and Advanced Materials Center, Gdansk University of Technology, 80-233, Gdańsk, Ul. Narutowicza 11/12, Poland*

[b] *Faculty of Materials Science and Ceramics, AGH University of Science and Technology, Al. A. Mickiewicza 30, 30-059, Kraków, Poland*

[c] *Department of Materials and Mineral Resources Engineering, National Taipei University of Technology, 1, Sec. 3, Zhongxiao E. Rd., Taipei, 106, Taiwan*

[d] *Faculty of Electronics, Telecommunications and Informatics and Advanced Materials Center, Gdansk University of Technology, 80-233, Gdańsk, Ul. Narutowicza 11/12, Poland*

HIGHLIGHTS

- CeO_2-based catalysts were prepared by cyclodextrin-assisted wet impregnation.
- The addition of cyclodextrin resulted in smaller metal nanoparticles of high dispersity.
- The Ni- and Co-containing samples resulted in high CH_4 yields at high temperature.
- Prepared catalysts can be applied in SOEC for CO_2 methanation.

GRAPHICAL ABSTRACT

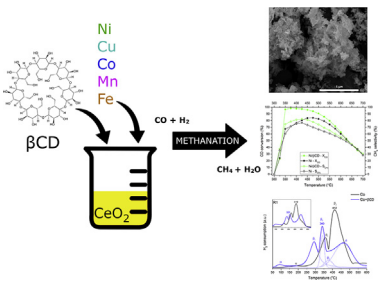

ARTICLE INFO

Article history:
Received 22 July 2021
Received in revised form
20 October 2021
Accepted 20 October 2021
Available online xxx

ABSTRACT

The aim of this work was to prepare and examine the catalytic activity of nanometric CeO_2 decorated with transition metal oxides – Ni, Co, Cu, Fe and Mn – towards a high-temperature methanation process under SOEC CO_2/H_2O simulated co-electrolysis conditions. Samples were prepared using the wet impregnation method via the conventional process and with the addition of native cyclodextrin. The influence of β-cyclodextrin (βCD) onto the size, dispersion and integration of the obtained metal nanoparticles was investigated. The differences between the catalysts' reducibility revealed that samples prepared from βCD-containing solutions, in most cases, resulted in the creation of smaller Me_xO_y

* *Corresponding author.*
E-mail address: patryk.blaszczak@pg.edu.pl (P. Błaszczak).

https://doi.org/10.1016/j.ijhydene.2021.10.144

Please cite this article as: Błaszczak P et al., Preparation of methanation catalysts for high temperature SOEC by β-cyclodextrin-assisted impregnation of nano-CeO_2 with transition metal oxides, International Journal of Hydrogen Energy, https://doi.org/10.1016/j.ijhydene.2021.10.144

Keywords:
Catalyst
Methanation
Transition metals
SOEC
β-cyclodextrin

NPs on the surface of the substrate material compared to those prepared using traditional nitrate solutions. The samples containing Ni and Co were the only ones that observably catalysed methane synthesis. The high dispersion and integration of NPs prepared via the proposed synthesis route resulted in increased catalytic activity and enhanced stability, which was most pronounced for the Co-impregnated sample. The methane production peak for Ni-βCD/CeO_2 at 375 °C was characterised by nearly 99% CO conversion and 80% selectivity towards CH_4 production. Co-βCD/CeO_2 reached 84% CO conversion and almost 60% methane selectivity at 450 °C. The usage of CeO_2 coupled with βCD for the preparation of catalysts for high-temperature methane synthesis for use in SOECs gave promising results for further application.

Introduction

The increasing demand for energy and fuel is having a significant deleterious impact on the natural environment due to the increasing CO_2 content in the atmosphere. Counteracting these environmental changes leads us towards attempts at reducing the CO_2 emission rate by e.g., capturing and reusing it in industrial processes and increasing the share of renewable energy sources. The conversion of carbon dioxide into various potentially useful products via electrolysis is one of the possibilities. Besides mitigating global warming caused by greenhouse gases emissions, such a strategy can bring extra benefits in the field of energy storage and transfer [1]. Solid oxide electrolysis cells (SOECs) are electrochemical devices consisting of a fuel electrode (cathode) and an air electrode (anode) separated by a nonpermeable, solid electrolyte. When water is applied as a fuel, its vapour comes into contact with the electrode surface and is reduced to hydrogen and an oxide ion. The reaction takes place at a triple phase boundary (TPB) where the electrolyte, gas phase, and the cathode material meet together. The hydrogen is collected from the cathode surface, and the oxide ion migrates into the cell, through the electrolyte and towards anode's surface where it is oxidised to molecular oxygen and the electrons are recirculated. It is also possible to carry out parallel electrolysis processes using the same cathode by the so-called co-electrolysis process. When carbon dioxide is used as a secondary type of fuel, its molecules can be decomposed to form carbon monoxide and an oxide ion. In such a case, the production of an industrially valuable mixture of hydrogen and carbon monoxide named 'syngas' occurs simultaneously. These gaseous fuel components and products of electrolysis can further react to form hydrocarbon fuels and in this way to even increase the energy conversion efficiency of the system. Among the possible reactions, methanation is thermodynamically favourable. In the case of CO_2 methanation, despite the concerns over the exact reaction route, the hydrogenation occurs according to the process expressed by Eq. (1). The carbon monoxide that is supplied or in situ produced (e.g. in a SOEC) is converted to methane (Eq. (2)) through a dissociative mechanism. The associative mechanism of methanation is preferred at high H_2 concentrations [2].

$$CO_2 + 4H_2 \rightarrow CH_4 + 2H_2O \left(\Delta H_{298} = -165\ kJ\ mol^{-1}\right) \quad (1)$$

$$CO + 3H_2 \rightarrow CH_4 + H_2O \left(\Delta H_{298} = -206\ kJ\ mol^{-1}\right) \quad (2)$$

$$CO + H_2O \rightarrow CO_2 + H_2 \left(\Delta H_{298} = -41\ kJ\ mol^{-1}\right) \quad (3)$$

However, as the process is highly exothermic, the usage of catalysts with appreciable activity is recommended [3]. Moreover, methanation is favoured at low temperatures and significantly limited at high temperatures [4], which is in contradiction with the high-temperature regime of SOEC operation. Another fact that should be taken into account is that water produced during the methanation, and that which is present at the fuel electrode of the SOEC will react with carbon monoxide to form carbon dioxide and hydrogen via the water-gas shift (WGS) reaction (Eq. (3)). In the working range of the SOEC the reverse reaction would proceed resulting in transformation of CO_2 into CO by reacting it with H_2 coming from water electrolysis. In that case, the CO_2 conversion into CO can follow two parallel reactions – reverse WGS and SOEC CO_2 electrolysis [5].

All of these facts indicate a very complex process of simultaneous H_2O/CO_2 electrolysis and methanation in a SOEC system. To improve the system efficiency and to increase the methanation during SOEC operation, the usage of proper methanation catalysts is highly desired. Those based on the VIII group metals are known for their high activity and stability [3,6]. However, the price of the active noble metals is one of the main factors that prevents methanation being used on an industrial scale. Therefore, cheaper compounds with a beneficial role are added to the catalyst. Among them, one may find promoters such as VO_x, MgO and La_2O_3, which affect the electron mobility, crystal texture, metal dispersion, and thermal stability of the catalysts [3]. As a result, they can provide some anti-sintering [7] and anti-coking [8] properties, as well as increased sulphur poisoning resistance [9] of the material. Another strategy is to use cerium (IV) oxide, which is a widely investigated material for photocatalysts [10], in the water splitting process [11], reforming processes [12] and as a fuel electrode and electrolyte in SOEC cells. The outstanding oxygen-storage ability associated with the easy conversion between the Ce^{4+} and Ce^{3+} oxidation states in CeO_2-based

compounds make them superior supports in many chemical processes [13]. Furthermore, they provide high chemical and thermal resistance, inhibit coke formation and promote the metal dispersion with simultaneous anti-sintering features [14,15]. Therefore, combining highly active metallic nanoparticles with advantageous ceria support seems to be an interesting system in the implementation of an active, stable, and relatively cheap catalyst for the methanation process in SOEC. It is especially interesting as SOECs and state-of-the-art catalysts have mostly been studied for effective syngas production, not for methanation [16,17]. Additional combined systems have been proposed for effective methanation using an external methanizer.

Several examples of selected catalysts for CO conversion to methane, based on CeO_2, are presented in Table 1. It shows that ceria-based catalysts with metal additives show promising properties for the methanation process, but these experiments were performed in methanation reactors and at relatively low temperatures (300–450 °C). At the higher temperatures (600–800 °C) at which a SOEC can be operated efficiently, reports on the successful application of catalysts for the methanation reaction are still lacking.

In this work, in contrast to most catalyst studies, a high-temperature catalyst for direct methanation in a SOEC chamber was investigated. Catalyst candidates based on metal-ceria composites were sought. Namely, several transition metals (Ni, Co, Cu, Fe, Mn) were deposited on commercially available CeO_2 using the wet impregnation method with the addition of β-cyclodextrin. Although proper studies over this group of materials are still missing, based on the literature reports [24–26], it was expected that this approach would result in obtaining smaller metallic nanoparticles (higher active surface area for catalytic reactions) coupled with strongly active CeO_2 substrate and prolonged catalyst lifespan under working conditions. The total amount of deposited metals was set to 10 wt%. The catalytic activity for performing the methanation reaction under a simulated SOEC working atmosphere consisting of (in the ideal case) syngas and water vapour was evaluated. The highest methane yields were obtained for the Ni- and Co–CeO_2 samples prepared with the addition of β-cyclodextrin with a low degradation rate during long-term stability tests.

Experimental

Catalysts preparation

All catalysts were prepared by the wet impregnation method of a nanometric CeO_2 substrate (99.5%, Alfa Aesar, particle diameter: 15–30 nm, SSA: 30–50 m^2g^{-1}). Appropriate amounts of transition metal nitrates – namely, $Ni(NO_3)_2 \cdot 6H_2O$ (99.9%, Merck), $Co(NO_3)_2 \cdot 6H_2O$ (99.9%, Merck), $Cu(NO_3)_2 \cdot 6H_2O$ (99.9%, Merck), $Mn(NO_3)_2 \cdot 4H_2O$ (99%, Merck), and $Fe(NO_3)_3 \cdot 9H_2O$ (99.95%, Merck) – were dissolved in 10 vol% EtOH in DI solvent to create 0.2 M solutions. Subsequently, solutions with β-cyclodextrin (βCD, ≥97%, SigmaAldrich) as a coordinating/capping agent were prepared by the addition of 0.05 mol βCD per 1 mol cations and were stirred at room temperature until completely clear. Each solution was then added to dry CeO_2 nanopowder to finally obtain 10 wt% metal content (concerning the Me^0 form) in the catalyst. The slurry was then evaporated with constant stirring at 90 °C until a highly viscous paste formed. After drying at 120 °C for 12 h, the obtained solid was ground using a mortar, transferred into an alumina crucible and sintered at 400 °C for 4 h under an air atmosphere to decompose the nitrates and remove the organic residue.

Characterisation techniques

Following the BET isotherm model, the surface area was measured using the N_2 adsorption technique (Quantachrome, NovaTouch LX1). The samples were degassed prior to sorption measurement at 300 °C for 3 h in a high vacuum. Diffraction patterns of impregnated catalysts were collected using a Bruker D2 PHASER XE-T with a Cu-Kα radiation source. Temperature programmed reduction (TPR) and Temperature Programmed Oxidation (TPO) tests were carried out in an AutoChem II 2920 (Micromeritics, TCD detector) under 40 $mLmin^{-1}$ stream of 5% v/v H_2 in Ar and 2% v/v O_2 in Ar, respectively. The tests were carried out from 100 up to 900 °C with a 10 °C min^{-1} temperature increase rate to examine the reducibility and substrate integration of the prepared metal oxide nanoparticles at the surface of nano-CeO_2. Two reduction cycles were performed each time to deliver more reliable reduction profiles and to determine the tendency of the metal oxides' nanoparticles to grow after oxidation. The morphology of the prepared powders was examined using a FEI Quanta FEG 250 scanning electron microscope. TEM imaging of the catalysts was performed using JEOL 2100F (Tokyo, Japan) microscope operating at 200 kV coupled with energy dispersive microscopy (EDS, Oxford Instruments, UK).

Catalytic test set-up

The measurement of the catalytic activity was performed at atmospheric pressure using a fixed bed reactor. The unit consisted of two connected furnaces. One was used to create water vapour by mixing a hydrogen-oxygen mixture at 700 °C in the presence of a Pt catalyst. The second was the main

Table 1 – Exemplary catalysts containing CeO_2 for efficient methanation.

Catalyst composition [wt.%]	GHSV [ml g^{-1} h^{-1}]	CO conversion [%]	Selectivity to CH_4 [%]	Temperature [°C]	Ref
15% Ni/CeO_2	150,000	98	99	300	[18]
10% Ni/CeO_2	60,000	99	98	300	[19]
15% Ni/CeO_2	10,000	100	84	350	[20]
5.2% Ni/CeO_2	60,000	90	78	450	[21]
30% Ni/10% Ce/Al_2O_3 (xerogel)	8160	91	50	240	[22]
2% Ru/γ-Al_2O_3	3000	98	85	400	[23]

Please cite this article as: Błaszczak P et al., Preparation of methanation catalysts for high temperature SOEC by β-cyclodextrin-assisted impregnation of nano-CeO_2 with transition metal oxides, International Journal of Hydrogen Energy, https://doi.org/10.1016/j.ijhydene.2021.10.144

reaction chamber with a 4 mm inner diameter quartz tube reactor. Water vapour mixed with syngas stream was fed into the reactor to simulate the conditions occurring at the working electrode of a SOEC during the process of CO_2 and H_2O co-electrolysis. The inlet mixture was composed of 80 vol% syngas (CO/H_2 1:3) and 20 vol% water vapour. The composition was chosen based on methanation reaction thermodynamic equilibrium calculations performed using the HSC Chemistry™ software from Outotec. The chosen inlet gas mixture was meant to produce the highest possible methane yield and no carbon accumulates while performing the catalytic tests. This simplified approach was applied to examine and predict the behaviour of each transition metal as a methanation catalyst under ideal, simulated conditions of a working SOEC [27].

The tendency of catalysts to limit SOEC efficiency by empowering CO_2 production was also discussed. Hydrogen was supplied from the electrolyser while other gases were provided by Air Liquide with purity over 99.9%. The outcoming gases were analysed using the FTIR-based measuring unit described in our previous works [28]. Briefly, it consisted of a FTIR spectrophotometer (PerkinElmer Spectrum 100) with a heated 10 cm path length gas sample cell (60 °C) equipped with ZnSe optical windows, flow meters for controlling the inlet/outlet gas stream flow rates and a cold trap followed by Nafion dryer tubing for complete water vapour removal. The concentration of the considered exhaust gases, which are CO, CO_2 and CH_4, was measured by integration of chosen parts of received spectra and calibration curves specially designated for our set-up. The calibration data was obtained using high purity (5N5) mixtures of the gases and the spectra integration was performed at 3760-3520 cm^{-1} for CO_2, 2226-2143 cm^{-1} for CO, and 3250-2650 cm^{-1} for CH_4, respectively. The flow path between the reactor and measurement point was maximally reduced to ensure immediate response despite the volume change of the gas during the reaction.

Experimental procedure and test conditions

The reactor quartz tube was each time filled with 100 mg of catalyst mixed properly with nonporous alumina carrier balls (99% Al_2O_3, Ø 1 mm) to ensure a free flow of reactants and products as well as even heat distribution throughout the catalyst bed. The volume of the bed was maintained the same for each test. Quartz wool was introduced on both ends to maintain good dispersion of the gas mixture and ensure that the catalyst bed stays in the central part of the reactor. The whole unit was thermally insulated to minimise temperature fluctuations. Prior to each measurement, the catalyst was activated using imitated conditions of SOEC reduction: under H_2 (24 ml min^{-1}) for 2 h at 800 °C. After cooling to 700 °C, the reactants were introduced into the feeding stream and the composition of the outlet gases was examined every 25 °C with 60 min equilibration time at each step. The syngas was passed through the catalyst bed at a total flow rate of 27.4 mL_{STP} min^{-1} (16,440 mL_{STP} g_{cat}^{-1} h^{-1}, GHSV = 4443 h^{-1}). The spectra for the concentration calculations were collected every 5 min in the range of 4000–450 cm^{-1} using 5 accumulations (4 cm^{-1} spectral resolution). Prior to each test, a leak check was performed to ensure a good seal. Long-term stability measurements were performed for the selected samples at 700 °C using an identical feeding mixture and set-up for 24 h. Finally, the tested catalysts underwent the same catalytic test run to further determine the high-temperature ageing effects during the mentioned 24 h hold.

The quality of the prepared powder for efficient methane production was determined based on the CO conversion (X_{CO}), CH_4/CO_2 yields (Y_i) and selectivities (S_i) obtained from the measured molar flow values. The given parameters were calculated using Eqs. (1)–(5) [27].

$$X_{CO}(\%) = \frac{\dot{n}_{CH_4}^{out} + \dot{n}_{CO_2}^{out}}{\dot{n}_{CH_4}^{out} + \dot{n}_{CO}^{out} + \dot{n}_{CO_2}^{out}} \times 100 \quad (4)$$

$$S_{CH_4}(\%) = \frac{\dot{n}_{CH_4}^{out}}{\dot{n}_{CH_4}^{out} + \dot{n}_{CO_2}^{out}} \times 100 \quad (5)$$

$$S_{CO_2}(\%) = \frac{\dot{n}_{CO_2}^{out}}{\dot{n}_{CH_4}^{out} + \dot{n}_{CO_2}^{out}} \times 100 \quad (6)$$

$$Y_{CH_4}(\%) = \frac{X_{CO} \times S_{CH_4}}{100} \quad (7)$$

$$Y_{CO_2}(\%) = \frac{X_{CO} \times S_{CO_2}}{100} \quad (8)$$

where: $\dot{n}_i^{out}$ is the molar flow rate of a specified gas at the outlet of the reactor.

In addition to the catalytic coefficients, the analysis of nonequilibrium reaction quotients (Q_r) was performed. To estimate the behaviour of the proposed reactions undergoing during the methanation, the Q_r values were calculated as a ratio of the nonequilibrium constant and the equilibrium constant for a specific reaction. The Q_r aids is determining the momentary direction of the selected reaction and gives an overall view on the kinetics of the considered process. The more detailed procedure of Q_r calculation and interpretation can be found in our previous work on biogas reforming in SOFC [28]. Briefly, the value of Q_r equal to 1 indicates that the reaction is at its thermodynamic equilibrium. It is approved that the value $Q_r > 10^3$ stands for the existence of mostly products, while $Q_r < 10^{-3}$ indicates that mostly reactants are present in the reaction area. In the intermediate range, the significant number of products and reactants is visible. The Q_r values were calculated vs. reaction temperature. The theoretical values of the equilibrium constants were derived from HSC Chemistry software.

Results

Preliminary results discussion

Concerning the observed conversion of CO into methane over the prepared catalysts, providing some preliminary information is worthwhile. Any conversion of reactant gases was unnoticeable below 200 °C irrespective of the catalyst used. For some of the samples, a small amount of the higher hydrocarbons, namely C_2H_6, were detected below 300 °C. In those cases, the CH_4 concentration was calculated using a different spectrum range (1400–1100 cm^{-1}) as methane and

Please cite this article as: Błaszczak P et al., Preparation of methanation catalysts for high temperature SOEC by β-cyclodextrin-assisted impregnation of nano-CeO_2 with transition metal oxides, International Journal of Hydrogen Energy, https://doi.org/10.1016/j.ijhydene.2021.10.144

ethane spectral lines overlap in a pristine integration range and by creating superposition alters the concentration results. The produced ethane quantities were low and will not be considered in this study.

All thermodynamic equilibrium data for the proposed reaction conditions were calculated using the HSC Chemistry™ software (Outotec, Finland).

Phase composition of the catalysts

Prior to catalytic tests, all of the synthesised powders were carefully characterised to determine the influence of β-cyclodextrin on the final product. The comparative XRD patterns of the prepared metal/CeO_2 catalysts are presented in Fig. 1. The powders consisted of two oxide phases, except for the Fe-impregnated sample. The most intensive peaks were attributed to cubic CeO_2 (*Fm-3m*) according to the included database pattern (see Fig. 1 bottom). The broadening comes from the nanometric nature of the support used. The XRD patterns were stacked to present the difference between catalysts prepared using a conventional method and the βCD-assisted impregnation route. Generally speaking, the peaks assigned to transition metal oxides were of relatively low intensity and strongly broadened. In fact, those could be easily distinguished from the CeO_2 peaks for samples where the βCD additive was omitted. In other cases, the introduction of the βCD capping agent into the precursor solutions resulted in even broader and hardly visible peaks. This implies that the addition of βCD caused an increase in metal dispersion over the support surface and increased the tendency for the creation of smaller crystallites (nanoparticles) [29,30]. The sizes of the metal oxide clusters were not estimated using Scherrer's equation as the high dispersion and low metal loading would give unreliable results. For the Fe-impregnated sample, the reflection coming from Fe species were not visible, most probably due to the high dispersion of nanoparticles, formation of an amorphous structure and/or fluorescence under Cu anode radiation.

To examine the possible formation of the solid solution between the metal oxides and CeO_2, the lattice constant was obtained using the Rietveld refining method. A slight deviation in the impregnated nano-CeO_2 lattice constant was observed from 5.408 Å for pure unmodified ceria. The lattice parameters of the impregnated CeO_2 are presented in Table 2 with the corresponding GOF factors. The obtained values pointed towards the possible creation of a solid solution between an active metal oxide and ceria support. The nanoparticles seem to interact with the support material by the corresponding CeO_2-doped interlayer as the transition metals can dissolve into the ceria lattice to some extent. Even though minor changes were noticed for different impregnated samples, the addition of the βCD capping agent resulted in a slightly more intensive decrease of the lattice parameter. This effect can be mainly attributed to the stronger reduction of the Me_xO_y size by the addition of βCD as well as the higher amount of existing interfacial solid solution. The higher dispersion and integration were achieved due to the interactions between the βCD and metal cations resulting in the creation and decomposition of the inclusion complexes. According to the studies of M. Najafpour et al. [24] on Mn-cyclodextrin complexes it was concluded that strong interaction between the Mn cations and oligosaccharide ring led to formation of well dispersed nanoparticles of metal oxide. At the same time the research of H. Liu et al. [25] revealed that small addition of the CD ensured high Ni dispersion over SBA-15 substrate. The peaks observed in mass spectrometer for $Ni(NO_3)_2$-CD mixtures were attributed to the formation of various Ni^{2+}CD and NO_3^-CD complexes. The ability of β-CD to encapsulate the Ni ions and to evenly distribute NO_3^- via hydrogen bonds using outer OH^- groups is the key to prevent the sintering of the Ni nanoparticles during calcination step.

The smaller nanoparticles are keener on creating stronger interactions with the support due to their high surface energy potential. This synergetic effect between the size reduction and heavy coupling at the active metal/support interface is highly desired. Smaller metal particles guarantee a higher catalytically active surface area, while the existence of a mixed interlayer can increase the overall efficiency and stability of the catalyst. On the other hand, the conventional thermal

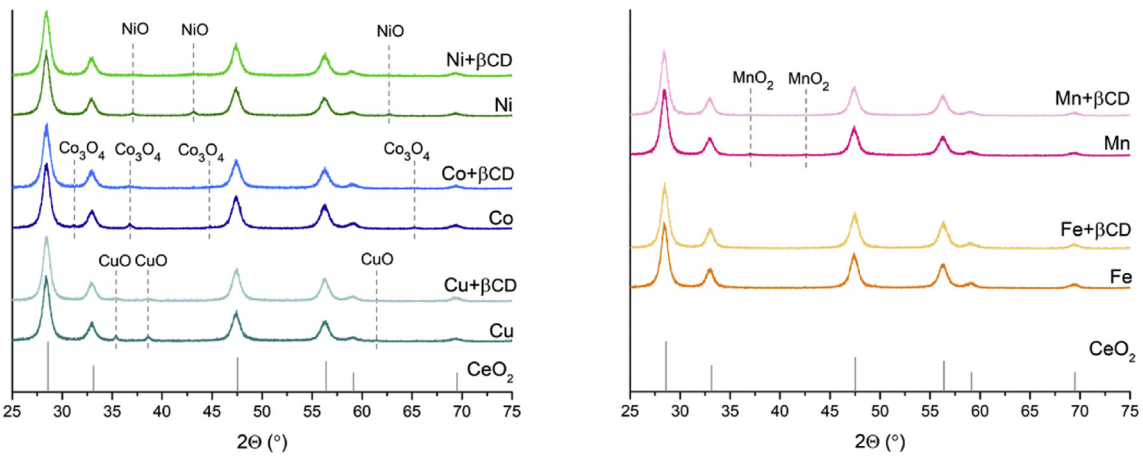

Fig. 1 – XRD patterns of CeO_2 support impregnated with 10 wt% metal content.

Please cite this article as: Błaszczak P et al., Preparation of methanation catalysts for high temperature SOEC by β-cyclodextrin-assisted impregnation of nano-CeO_2 with transition metal oxides, International Journal of Hydrogen Energy, https://doi.org/10.1016/j.ijhydene.2021.10.144

Table 2 – Lattice parameters of the pure CeO_2 support powder and impregnated catalysts.

	CeO_2	Ni		Co		Cu		Mn		Fe	
		pure	βCD	pure	βCD	pure	βCD	pure	βCD	pure	βCD
Lattice parameter (a = b = c) (Å)	5.408	5.403	5.401	5.405	5.401	5.402	5.401	5.402	5.400	5.405	5.399
GOF	1.68	1.40	1.23	1.24	1.32	1.27	1.22	1.53	1.29	1.21	1.49

calcination can cause the nanoparticles to create a broad diffused interfacial region, limiting the reaction's available catalytic centres [31]. A compromise between nanoparticle integration and reducible surface needs to be achieved. To determine the behaviour of the catalysts during activation, H_2-TPR measurements were performed.

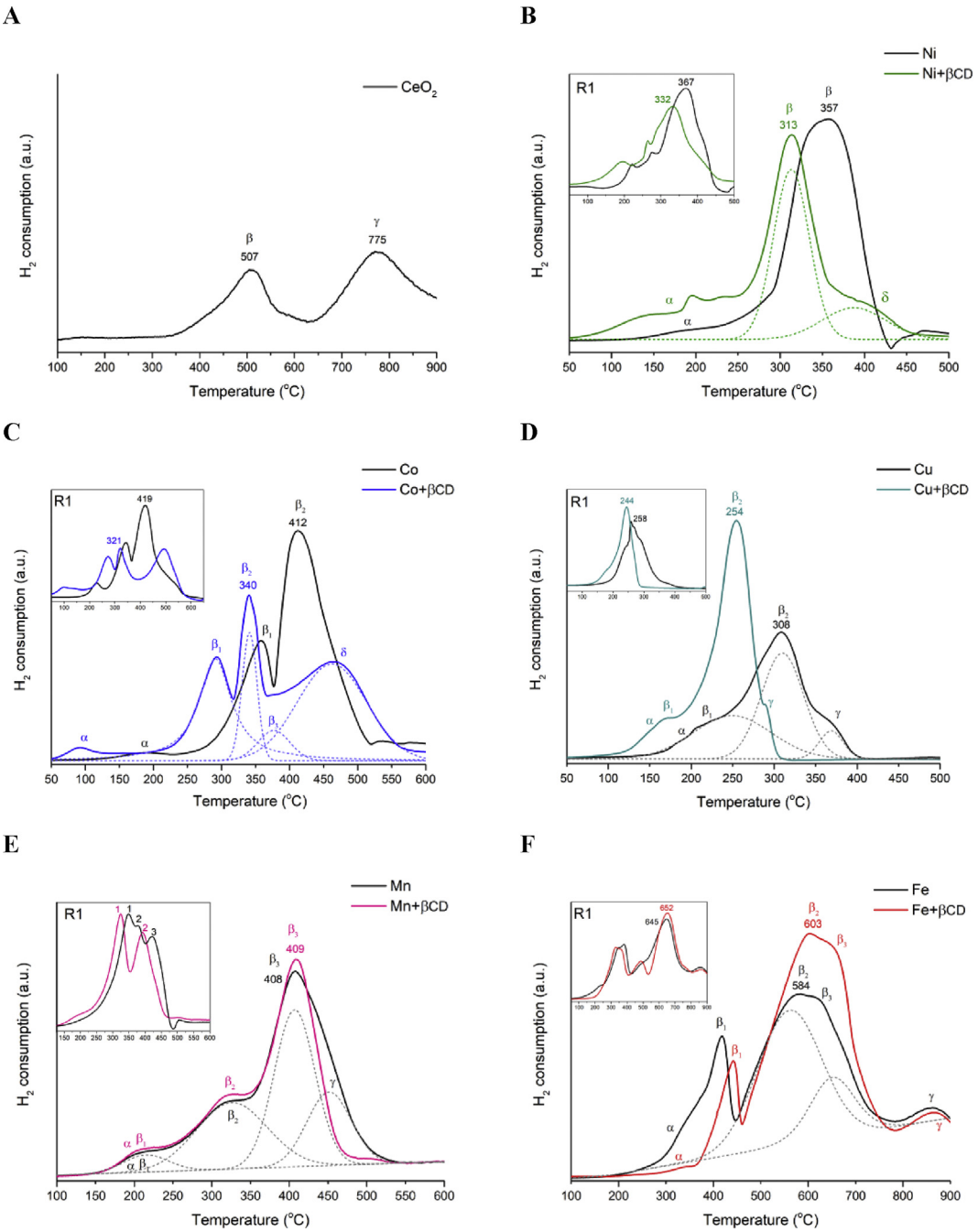

Fig. 2 – TPR profiles of the CeO_2 impregnated catalysts. Inset R1 shows the first reduction cycle profile.

Please cite this article as: Błaszczak P et al., Preparation of methanation catalysts for high temperature SOEC by β-cyclodextrin-assisted impregnation of nano-CeO_2 with transition metal oxides, International Journal of Hydrogen Energy, https://doi.org/10.1016/j.ijhydene.2021.10.144

Reducibility of the catalysts

To examine the reducibility of the prepared catalyst powders and define the reduction route of the transition metal oxides supported on the CeO_2 substrate, series of H_2-TPR measurements were performed after degassing and cleaning in a stream of He. Each test consisted of two reduction cycles with an intermediate oxidation run to reveal the metal's stability and tendency to agglomerate while redox cycling. The second reduction runs were selected as representative results as the samples were free of most surface impurities after the O_2/He oxidation step and are shown in Fig. 2. The first reduction profiles were also included in the graphs (R1 insets). The TPR profile of the pristine CeO_2 support (Fig. 2A) is characterised by the bimodal curve with two easily distinguishable peaks located at 507 °C and 775 °C indicated as β and γ, respectively. This effect is observable for ultrafine nanometric ceria particles with an intermediate specific surface area of rather low internal porosity development. The first peak (β) at lower temperatures comes from the surface reduction of CeO_2. It is followed by the second peak (γ) attributed to reduction with oxygen supplied from the bulk solid [32,33]. The lower temperature of the bulk reduction results from the highly developed surface area and the porosity of the nano-CeO_2 support that was used. The relatively high intensity of the consumption peak at 507 °C is due to the high concentration of surface oxygen species (O^{2-} and O^{-}) [34]. Also, the nanocrystallinity of the ceria support is the main reason for the lower temperature bulk reduction. The concentration of surface oxygen, oxygen vacancies, and Ce^{3+} ions can be a couple of magnitudes higher when reducing the nanoparticles' size. As an example, Xu et al. [35] revealed a significant decrease in bulk reduction peak intensity when the size of the CeO_2 decreased from 30 to 4.4 nm. At the same time, Zhuo et al. [36] stated that the concentration of oxygen vacancies was higher by a magnitude of two for 4 nm CeO_2 than for 60 nm CeO_2.

Comparing the TPR profiles of the nickel-, copper- and cobalt-impregnated CeO_2 samples revealed big differences in the reducibility of the metal oxides prepared using the conventional and βCD-assisted methods. For all of the mentioned oxides, the main reduction peaks were shifted towards lower temperatures, which stands for the creation of smaller and strongly dispersed nanoparticles of metal oxides over the surface of the CeO_2. The effect is visible during the first as well as second reduction cycle with no or a slight change of main reduction peak temperature. The temperature shift for Ni-, Co- and Cu-impregnated samples is especially suppressed, and additional oxidation most probably causes even structure refining and recrystallisation. That represents quite high stability towards cycling redox treatment and a low tendency of the metal NPs to migrate and coalesce. For the latter samples, namely Mn- and Fe—CeO_2, the differences resulting from the βCD additive are not that pronounced. For all of the samples, the α region in the TPR profiles was indicated near 200 °C. According to the literature, it was fully attributed to the reduction of surface-active adsorbed oxygen species. It is also generally accepted that incorporating a transition metal dopant into a ceria lattice also creates easily reducible oxygen species by the generation of oxygen vacancies [37–40].

In the TPR profile of nickel impregnated ceria (Fig. 2B), the main H_2 consumption peak (β) was attributed to the reduction of free, bulk NiO particles loosely integrated with the support [38,41]. In the sample with no βCD, this one process is the main step in the catalyst reduction occurring at 357 °C. Compared to the conventionally prepared catalyst, the Ni-βCD/CeO_2 was characterised by a shift in the temperature of β to lower values and the existence of one additional H_2 consumption peak around 400 °C, namely δ. This process can be assigned to the reduction of highly dispersed Ni strongly integrated with the CeO_2 by Ni—O—Ce interactions and the creation of a solid solution interlayer [41–43]. The higher intensity of the α process and the observed δ peak proves that the addition of βCD improves the nickel dispersion and leads to the creation of intermediate compounds with CeO_2 by partial NiO dissolution. This issue will be discussed further in this paper.

The TPR profile of the βCD-assisted Co-impregnated CeO_2 (Fig. 2C) was much more complex than for conventionally prepared one and was deconvoluted into 5 different processes. The reduction behaviour of Co_3O_4 and the description of its reduction steps is rather controversial in the literature as the TPR profiles differ significantly depending on the preparation route, catalyst composition and level of Co dispersion. It is generally agreed that large particles of loosely integrated Co_3O_4 are reduced in a single step resulting in metallic Co^0. Depending on the dispersion, smaller particles that interact with ceria seem to undergo a reduction via a two-step process, including CoO creation [44]. The consumption peak designated as β_1 was attributed to the reduction of Co^{3+} to Co^{2+} in fully oxidised Co_3O_4 particles strongly integrated with the oxide support promoted by the interaction of the components, ascribed possibly to Co—O bond lengthening [45]. The intermediate temperature reduction peaks at 340 and 412 °C were indicated as β_2 for βCD-Co/CeO_2 and Co/CeO_2, respectively. Based on the peak description by Luo et al. [46] concerning studies of Co_3O_4/CeO_2 and Pd—Co_3O_4/CeO_2, the β_2 process was fully attributed to the direct reduction of independent Co_3O_4 to metallic Co. For the traditional nitrate solution method of preparation, this process was the most dominant. In the case of the catalysts impregnated using βCD, two additional peaks were identified in the TPR profile. The β_3 peak most probably stands for an intermediate step of reduction of loosely integrated CoO. It happens just before the reduction of strongly integrated Co^{2+} ions designated as the broad δ consumption peak around 460 °C [46,47]. The Co^{2+} ions embedded into the ceria support were harder to be reduced due to their stabilising effect on cobalt medium valence ions and high oxygen storage capacity [45,46]. Moreover, a phenomenon called hydrogen spillover, was most probably taking place during the H_2 treatment. Once the highly dispersed Co_3O_4 got reduced to Co^0, this new metallic phase acted as the dissociation centre for H_2 molecules. The hydrogen atoms promoted a reduction and caused shifting towards lower temperatures. The higher dispersion of cobalt oxide over the surface of ceria, resulted in triggering the effective reduction of strongly integrated Co^{2+} and of the support underneath by self-accelerating the H_2-oxide reaction [46,48,49].

Please cite this article as: Błaszczak P et al., Preparation of methanation catalysts for high temperature SOEC by β-cyclodextrin-assisted impregnation of nano-CeO_2 with transition metal oxides, International Journal of Hydrogen Energy, https://doi.org/10.1016/j.ijhydene.2021.10.144

Even though the integrated amounts of hydrogen uptake both for the samples with and without βCD additive were quite similar, additional experimental studies were undertaken in order to determine if the undoubtedly created solid solution of (NiO/Co_3O_4)–CeO_2 in the βCD-(Ni/Co)/CeO_2 catalysts lead to the confinement of a distinct amount of Ni/Co ions in the structure and as a result, lowering the final amount of active metal species after reduction. For this reason, the H_2-TPR measurements were performed using nanocrystalline 20 mol% Ni- or Co-doped CeO_2 prepared by the reversed microemulsion route. Briefly, two solutions were prepared: nonaqueous organic phase containing surfactant (Triton X-100) and aqueous one containing metal cations. The solutions were then mixed together to form a dispersion. The ceramic precursor powders were then precipitated using a tetraethylammonium hydroxide, centrifuged, washed and sintered at 500 °C under air atmosphere. The synthesis methods and complete description of the microstructure were published in our previous work [50]. The TPR profiles with corresponding before- and after-reduction XRD patterns of the $Ce_{0.8}Ni_{0.2}O_{2-\delta}$ and $Ce_{0.8}Co_{0.2}O_{2-\delta}$ are presented in Fig. 3. Both TPR profiles were divided into two regions: I) reduction of the surface and loosely integrated Me^{x+} species at lower temperatures, and II) removal of the ions strongly coupled with the support by (Ni/Co)–O–Ce interactions. The later one also corresponded to the reduction of Ce^{4+} ions most possibly accelerated by hydrogen spillover phenomena and/or NiO/Co_3O_4 highly dispersed in a solid solution. A slight lowering in the overall reduction temperature was noticed, especially for Co-doped CeO_2. This behaviour was previously described by other groups [51,52]. The Rietveld refining method was used to determine the lattice parameters of the Co/Ni-doped CeO_2 samples (based on the XRD patterns presented in Fig. 3 left). The corresponding lattice constants of the as-synthesised $Ce_{0.8}Ni_{0.2}O_{2-\delta}$ and $Ce_{0.8}Co_{0.2}O_{2-\delta}$ were 5.408 Å (GOF = 1.57) and 5.398 Å (GOF = 1.62), respectively. After the TPR measurements, the XRD pattern consisted of CeO_2 and the corresponding metallic phase. An increase in the CeO_2 lattice parameters was observed and equal to 5.415 Å for $Ce_{0.8}Ni_{0.2}O_{2-\delta}$ and 5.414 Å for $Ce_{0.8}Co_{0.2}O_{2-\delta}$, respectively. This change goes well with the unit cell parameter of 5.411 Å for pure microcrystalline ceria. This revealed the complete decomposition of the doped compounds into cermet composite during reduction.

Previous studies concerning the CuO_x-CeO_2 catalytic systems revealed that by forming the Cu–Ce interactions, a redox synergy of the final catalyst was promoted by using ceria as an active support. Both the CuO_x species and CeO_2 were more readily reducible than those components separately [53]. According to the H_2-TPR measurement of the Cu-impregnated CeO_2 (Fig. 2D), the profile was deconvoluted into three peaks, namely β_1, β_2, and γ. Based on the temperature ranges and the literature, the β_1 consumption peak was attributed to the reduction of small and highly dispersed CuO_x species. Simultaneously, the β_2 process was the reduction of Cu^{2+} ions integrated with the CeO_2 by the Cu-[O_x]-Ce interactions. The shoulder peak γ was highly pronounced for the catalyst conventionally impregnated without βCD additive and corresponded to the reduction of the bulk CuO particles visible in the XRD pattern (see Fig. 1.) [54–56]. The clear lowering of the reduction temperature and increase in the intensity of the β_2 peak confirmed the beneficial character of the βCD additive on increasing the dispersion, reducing the particle size and increasing the integration of CuO with the support. It is a crucial aspect from the point of view of catalysis.

The TPR profiles of the second reduction cycles of both Mn-impregnated catalysts were similar and typical for MnO_2 (Fig. 2E). The β_1, β_2 and β_3 consumption peaks were attributed to the reduction of MnO_2 to Mn_2O_3, Mn_2O_3 to Mn_3O_4, and Mn_3O_4 to MnO, respectively [57]. The bigger agglomerates of bulk Mn_3O_4 gave rise to the overlapping γ peak in the conventionally prepared Mn–CeO_2 catalyst. The MnO_2-altering properties of the βCD additive were observable only during the first reduction cycle (see Fig. 2. Mn R1 inset). The completely different shape of the TPR profile with two distinguishable peaks could be attributed to the following transitions: 1) Mn^{4+} to Mn^{3+}, and 2) Mn^{3+} to Mn^{2+}. This phenomena of omitting the intermediate state of Mn_3O_4 is observed in a highly nanometric MnO_2 structure characterised by a high specific surface area (SSA) [58,59]. The positive impact on the integration of manganese oxide with the βCD additive is too low to overcome the overall tendency of MnO

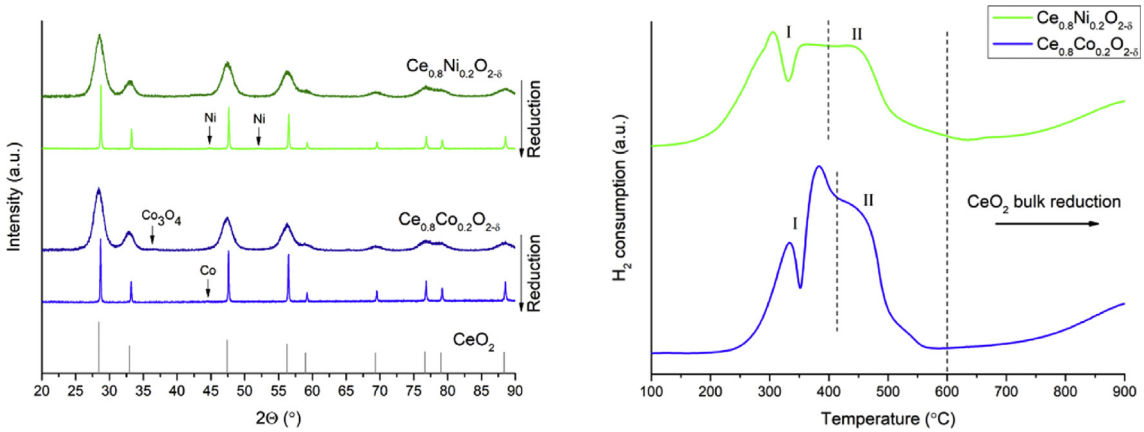

Fig. 3 – XRD patterns before/after reduction (left) and TPR profiles (right) of $Ce_{0.8}Ni_{0.2}O_{2-\delta}$ and $Ce_{0.8}Co_{0.2}O_2$. I – surface reduction and II – reduction of Ni and Co ions strongly integrated with the support.

Please cite this article as: Błaszczak P et al., Preparation of methanation catalysts for high temperature SOEC by β-cyclodextrin-assisted impregnation of nano-CeO_2 with transition metal oxides, International Journal of Hydrogen Energy, https://doi.org/10.1016/j.ijhydene.2021.10.144

towards agglomeration and sintering which limits its redox stability and catalytic activity.

The results of the H_2-TPR measurements of Fe-impregnated CeO_2 (Fig. 2F) were divided into four main stages besides adsorbed surface oxygen species reduction (α). The profiles of both Fe-containing samples were similar despite the addition of the βCD into the precursor solution. The reduction process was typical for Fe_2O_3 and widely described in the literature [60–62]. The β_1 consumption peak in the range of 350–450 °C was attributed to the reduction of Fe_2O_3 into Fe_3O_4. The following intermediate reduction steps β_2 and β_3 could be described as the overlapping reduction signals (see Fig. 2f) of Fe_2O_3 to FeO and FeO to Fe^0 transitions, respectively. Finally, the γ peak corresponded to the reduction of bulk clusters of FeO into metallic Fe.

The H_2-TPR experiment revealed that the βCD additive produces excellent microstructural changes mainly when Ni, Co, or Cu ions were used to impregnate the chosen nanometric CeO_2 support. The reduction of the nanoparticles' sizes is most probably a result of metal ions capping properties of the β-cyclodextrin. The cations are being captured inside the βCD macrocyclic ring of glucose units, increasing the metal ions' dispersity and limiting the agglomeration while sintering. Additionally, the burning cyclodextrin acts as a reducing agent that accelerates the metal oxide's creation and its slight dissolution into the surface layers of the partially reduced CeO_2 [63–65].

Microstructure and specific surface area (SSA)

The SSA and microstructure type are the catalyst's fundamental properties as those impact the final efficiency on the same level as the composition. The N_2 adsorption-desorption isotherm of the representative sample of βCD-Ni/CeO_2 is presented in Fig. S1. The isotherms for all of the samples were of the same shape. Based on the classification of the International Union of Pure and Applied Chemistry (IUPAC), all of them were type II isotherms, indicating that the catalysts have a developed amount of mesopores [66]. The isotherms were characterised by a H3-type hysteresis loop characteristic for samples containing irregular and open pores with good connectivity between intragranular pores. This microstructure guarantees good transport of the reactant gases [67]. The microstructures of βCD-Ni/CeO_2 and Ni/CeO_2 catalysts are presented in Fig. 4A. The TEM images coupled with μEDS analysis revealed that after the introduction of βCD into the precursor solution, the dispersion level of Ni over the support clearly increased. It is in agreement with the previously presented analysis of the TPR and XRD outcomes. Addition of cyclodextrin ensured good distribution of the guest ions over the sponge-like structure of nano-CeO_2 (see Fig. 4C). Possible formation of the mixed NiO–CeO_2 oxide was also identified, to some extent, using the HR-TEM image shown in Fig. 4B. The indicated bright spots of the image were determined to be (111) planes of pure cubic CeO_2 exhibiting interplanar distance of 3.1 Å. Presented values correspond well to the d-spacing found in the literature and Bragg law [68]. Interestingly, the interplanar distances of the congruent group of (111) planes measured within the region indicated in Fig. 4B were each time lower (2.9–3.1 Å) than for pure CeO_2. The alteration of interplanar distances towards lower values coupled with the results from μEDS may indicate the formation of the previously predicted Ni–O–Ce solid solution. As the transition metals possess the ability to dope the ceria lattice to some extent [50], this process occurred at the interface during the preparation step of the presented catalysts, changing the local interplanar distance due to the possible interdiffusion of Ce and Ni cations [69,70]. The formation of the surface Ni–O–Ce mixed oxide is considered an advantage when the catalyst is used in the methanation process [71]. Similar conclusions can be made for Co–CeO_2 catalyst series. The corresponding TEM images can be found in supplementary materials (Fig. S2).

The isotherm-based divagations over the microstructure were well reflected in the SEM images (Fig. 4.) of the impregnated catalyst. The structure of the catalysts was coral reef-like with a not easily distinguishable transition metal oxide phase. This was most probably due to high dispersion of metal followed by the formation of small

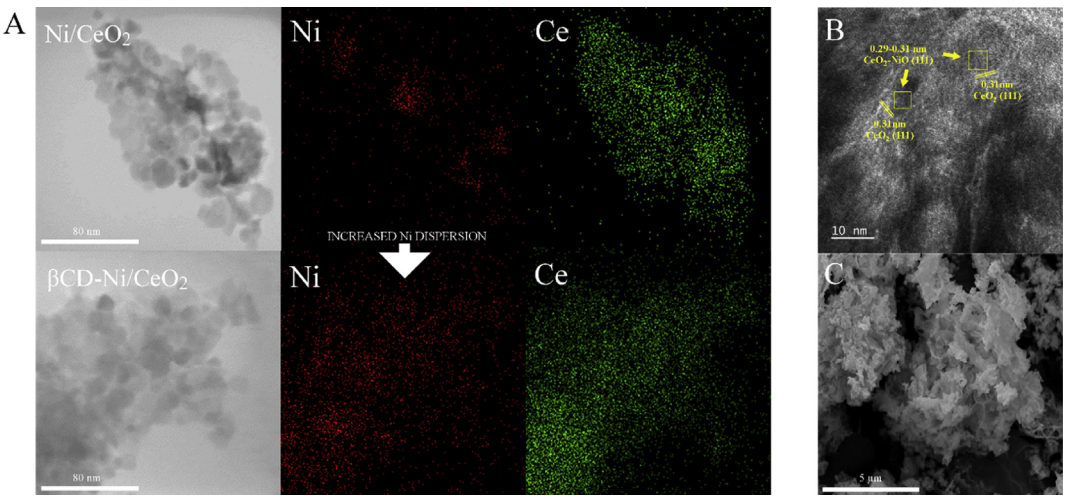

Fig. 4 – (A) TEM images with μEDS elemental analysis of Ni and Ce of βCD-Ni/CeO_2 and Ni/CeO_2 catalysts, (B) HR-TEM image of βCD-Ni/CeO_2 sample with indicated (111) interplanar distances and (C) SEM image of βCD-Ni/CeO_2.

Please cite this article as: Błaszczak P et al., Preparation of methanation catalysts for high temperature SOEC by β-cyclodextrin-assisted impregnation of nano-CeO_2 with transition metal oxides, International Journal of Hydrogen Energy, https://doi.org/10.1016/j.ijhydene.2021.10.144

Table 3 – BET specific surface area (SSA) and total pore volume of the prepared catalysts.

	CeO_2	Ni		Cu		Co		Mn		Fe	
		pure	βCD	pure	βCD	pure	βCD	pure	βCD	pure	βCD
BET surface area (m^2g^{-1})	35.5	52.1	55.4	49.8	60.6	57.0	61.1	52.7	54.4	70.0	69.8
Total pore volume ($10^{-1}cm^3g^{-1}$)	1.5	1.9	2.2	1.7	2.0	1.6	1.7	1.6	1.7	1.8	2.1

nanoparticles of low crystallinity. The specific surface areas (SSA) of the as-synthesised catalyst powders are collected in Table 3. It is clearly visible that all of the impregnated samples are characterised by higher SSA values compared to the pristine CeO_2 powder. The surface areas estimated for the prepared catalysts were in the range of 49.8–70 m^2g^{-1}. Except for the Fe-impregnated sample, they all exhibited a slightly higher surface area when βCD was added during the preparation process. This was caused by higher metal oxide dispersion. The effect of the βCD additive was most pronounced in the Cu-containing sample where the SSA increased from 49.8 to 60.6 m^2g^{-1}. This was caused by the fact that Cu^{2+} ions form the most long-lasting complexes with βCD which are also stabilised by NO_3^- groups. According to previous studies, Cu and Co complexes with βCD are much different than those of other transition metal salts, e.g., by altering the temperature decomposition [72,73]. This indicates that, especially in the case of the Cu- and Co-impregnated samples, the βCD allowed much smaller nanoparticles to be obtained, which is in agreement with the strong shift in the reduction maximum during the TPR tests in both cases. The effect of the cyclodextrin additive was rather poorly visible in the case of Mn- and Fe-impregnated samples. The highest values of SSA were observed for the Fe/CeO_2 catalyst. This would correspond well to the highly amorphous structure of Fe_2O_3 created on the CeO_2 support, which was obtained during low temperature (400 °C) sintering of the impregnated ceria. The total pore volumes varied between 1.6–2.2 × $10^{-1}cm^3g^{-1}$, where higher values were also found for the samples prepared using βCD.

Catalytic activity for CO conversion to methane

The catalytic activity of the samples was examined using fixed bed reactor and FTIR for analysis of the composition of the exhaust gases. The baseline consisted of the unmodified CeO_2 powder mixed with the alumina diluent media. No methane formation was observed. Visible methane formation was only noticed for two of the prepared catalyst samples, being the Ni- and Co-impregnated CeO_2. For the rest of the samples, the CH_4 concentration was significantly below 1%, and thus only the Ni- and Co-impregnated samples with/without βCD were taken into further consideration. The temperature-dependent CO conversion and CH_4 selectivity as well as CH_4/CO_2 yield values were calculated for the mentioned catalysts and are presented in Figs. 5 and 6 for the Ni- and Co-impregnated samples, respectively. For the Ni/CeO_2 catalysts, both the CO conversion and selectivity towards methane production were higher than for the Co/CeO_2 catalysts. This proves the high catalytic activity of Ni for the methanation reaction. The increase in the activity of the catalyst prepared with the assistance of the βCD was clearly noticeable concerning both CO conversion and CH_4 selectivity. The CO conversion reached 98.5% at 375 °C compared to around 71.4% for the catalyst prepared without the βCD additive (peaking at 475 °C in 84.4%). Better dispersion over and integration of the Ni nanoparticles with the CeO_2 surface ensured higher (625–350 °C) or similar (700–650 °C) efficiency of the Ni/βCD-CeO_2 catalyst concerning the CH_4 selectivity and CO conversion. When comparing the CH_4 yield of both Ni-containing catalysts, the one prepared using βCD reached 79.9%, while the other only reached 61.9%. Simultaneously, the CO_2 yield was calculated as the unwanted

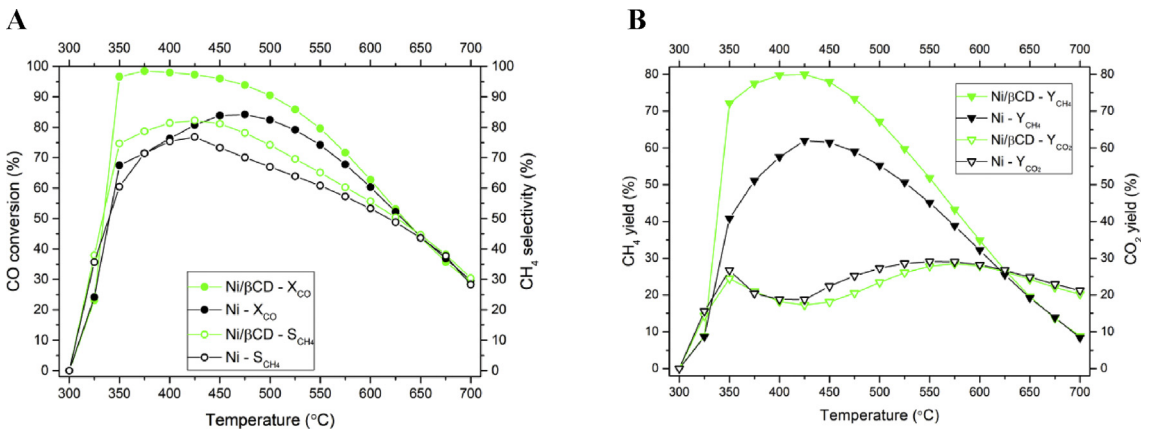

Fig. 5 – Catalytic performance of the Ni-impregnated CeO_2. a) CO conversions and CH_4 selectivities, and b) CH_4 and CO_2 yields.

Please cite this article as: Błaszczak P et al., Preparation of methanation catalysts for high temperature SOEC by β-cyclodextrin-assisted impregnation of nano-CeO_2 with transition metal oxides, International Journal of Hydrogen Energy, https://doi.org/10.1016/j.ijhydene.2021.10.144

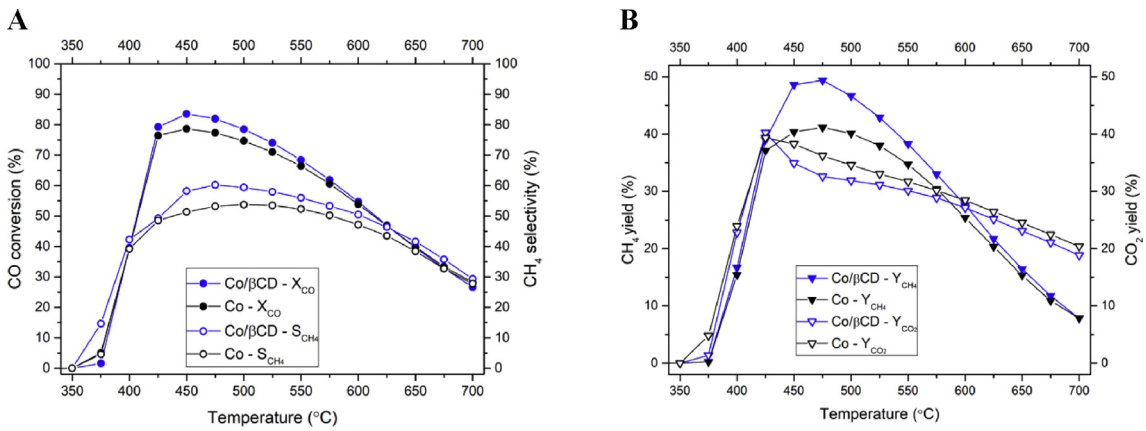

Fig. 6 – Catalytic performance of the Co-impregnated CeO_2. a) CO conversions and CH_4 selectivities, and b) CH_4 and CO_2 yields.

side reaction of WGS took place using up CO for CO_2 generation. In a working SOEC, CO_2 will be reduced into CO, so the catalyst reversing this process by reacting CO with H_2O is highly undesired. As can be seen in Fig. 5b, the CO_2 yields in both cases were similar, and regarding the higher CH_4 yield obtained for the Ni/βCD-CeO_2, it indicated the higher overall efficiency of that catalyst in the proposed set-up. According to the study of S. Tada et al. [74] indicated that Ni metal particles coupled with CeO_2 and properly pretreated are highly active towards CO_2 reduction to CO at the support-metal interface. The high activity of Ni is determined by lower reaction temperature to overcome the eight-electron CO_2 methanation kinetic energy barrier, which implies the higher yield according to thermodynamic equilibrium limitations. Even though the reaction pathways are still under debate, the metal-ceramic interface and small size of Ni nanoparticles are generally believed to be a key to the most efficient methanation [75,76]. The metallic Ni particles are sites for H_2 sorption and activation [75,77]. The creation of surface Ni–O–Ce solid solution of low stability under reducing condition allows to form extremely small nanoparticles of metal facilitating hydrogenation [71].

For the Co-impregnated catalyst samples, the effect of the βCD was slightly less pronounced, yet clearly noticeable. The CO conversion for the Co/βCD-CeO_2 peaked at 83.5% at 450 °C, while for the conventionally impregnated ceria, it reached 78.6% at the same temperature. The values of CH_4 selectivities presented in Fig. 6a revealed a slightly higher tendency for methane formation within the whole temperature range when Co/βCD-CeO_2 was tested. The addition of βCD to the precursor solution resulted in a higher CH_4 yield of the synthesised catalysts revealing a 20% improvement concerning the peak point. At the same time, the CO_2 formation was suppressed, as indicated by the lower CO_2 yield values obtained for the Co/βCD-CeO_2 catalyst. The Co usage in each test resulted in the methane production peaking at temperatures higher than when Ni-containing catalysts were characterised.

As methanation can take place even more efficiently in the lower temperature regions, more specific tests with a higher number of intermediate steps could be performed, but according to the predicted application of the catalyst in a SOEC, the low-temperature region is of lesser importance.

The ageing of the powders was performed for 24 h under the same feeding mixture at 700 °C. After 24 h, the powders underwent the same test run as previously to determine the changes in catalytic efficiency caused by deterioration of the catalyst, e.g., metal particles sintering, and vaporisation. The results for comparison of the catalysts' deactivation resistance are presented in Fig. 7. The value changes of the chosen catalytic indicators, namely, CO conversion, CH_4 yield, and CH_4 selectivity, are presented for the narrowed temperature range to increase the picture clarity and the higher importance of that temperature region concerning the future application in SOECs. The changes in parameter values were indicated for the selected temperatures in the form of Δ%. The values of conversion, yield and selectivity at thermodynamic equilibrium were introduced in Fig. 7 as a dashed line. The values of reaction quotient Q_r depending on the reaction temperature were presented in Fig. 8 for Ni- and Co-impregnated CeO_2 samples. For calculation of the reaction quotient, only CO/CO_2 methanation and WGS reactions were taken into account as the most important ones.

The highest CO conversion and CH_4 yield values following close the limitation arisen by thermodynamic equilibrium, especially at high temperatures, were obtained for the Ni/βCD-CeO_2 catalyst. The Ni catalyst prepared without addition of cyclodextrin in both cases was characterised by lower efficiency, however, the selectivity towards CH_4 generation was comparable in both samples. The selectivity change follows the simulated trend, but the deviation from the thermodynamic equilibrium values may be caused by the uncertainty of concentration measurement by FTIR and possibility of slight temperature gradient formation inside the reactor catalyst bed. In the case of Co impregnated samples, the differences were less pronounced, but indicated the positive influence of βCD addition. The Co–CeO_2 samples were each case farther away from obtaining the thermodynamic equilibrium values in comparison to Ni–CeO_2. In general, the catalytic measurements indicated that the methanation at high temperatures under the proposed conditions is mostly determined by the

Please cite this article as: Błaszczak P et al., Preparation of methanation catalysts for high temperature SOEC by β-cyclodextrin-assisted impregnation of nano-CeO_2 with transition metal oxides, International Journal of Hydrogen Energy, https://doi.org/10.1016/j.ijhydene.2021.10.144

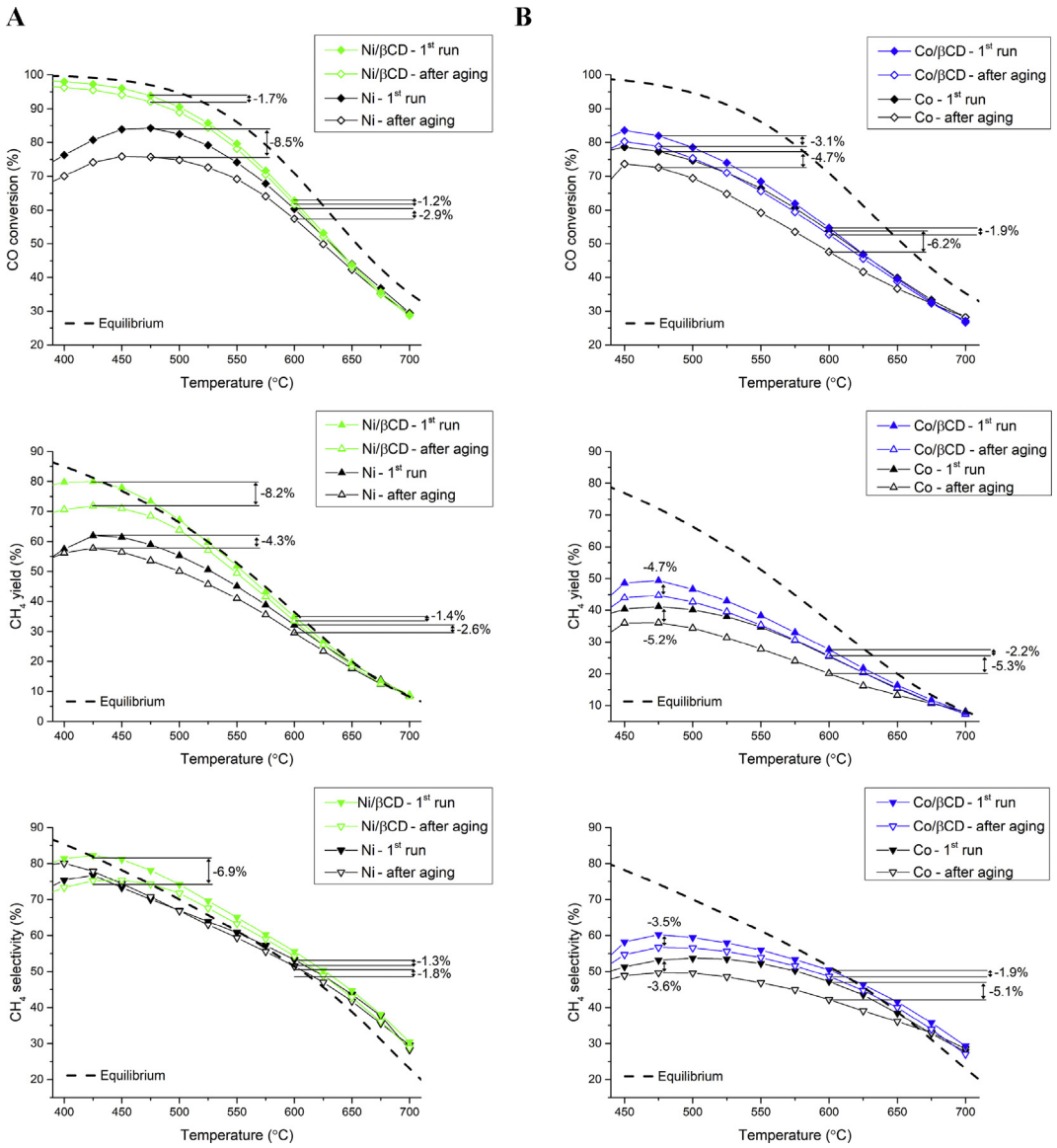

Fig. 7 – Change in catalytic parameters after 24 h of catalyst ageing at 700 °C. A) Ni-impregnated CeO_2, and B) Co-impregnated CeO_2. Dashed line indicates thermodynamic equilibrium values.

thermodynamic equilibrium and not the kinetics of the reaction itself.

Both of the catalysts did not deteriorate heavily during the 24 h hold at 700 °C. In fact, the usage of CeO_2 in nanometric form most probably limited the metals' tendency to agglomerate. In the end, the catalysts prepared using the βCD additive were characterised by a lower degradation level, especially for the Co-impregnated sample and Ni at high temperatures. The indicated changes in all of the parameters' values at 600 °C represent a much lower drop for the Co/βCD-CeO_2 and Ni/βCD-CeO_2 catalysts. The stability was clearly manifested for the Co/βCD-CeO_2 sample when both the low- and high-temperature regions were compared. This deterioration resistance was determined by the high integration of the Co with the CeO_2 support revealed during the H_2-TPR studies. Co metal by itself is known for lower tendency towards agglomeration and sintering than Ni. The stability of Co nanoparticles was even more enhanced by the βCD additive. Each time, a lower drop in values of the calculated parameters (CO conversion, CH_4 yield and CH_4 selectivity) was observed for the Co/βCD-CeO_2 catalyst. It reveals the significant influence of the native cyclodextrin addition on the final efficiency and stability of the catalyst.

The changes in catalytic parameter values varied depending on the reaction's temperature, generally producing higher drops in lower temperature regions. This is due to the higher efficiencies of the catalysts so even limited deterioration is clearly visible. For the Ni-impregnated samples, a significant difference was observed in the CO conversion value. Almost no change in conversion was noticed for the Ni/βCD-CeO_2, although, its deterioration was more pronounced in the case of the CH_4 yield and selectivity (see Fig. 7). Even after the slight deactivation, the overall efficiency stayed at a higher level than for the conventionally prepared samples. The higher

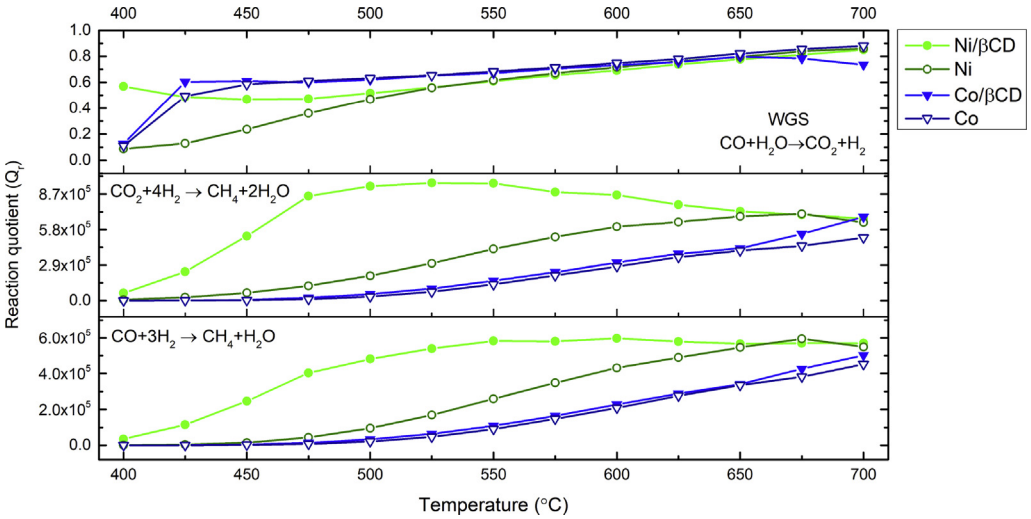

Fig. 8 – Reaction quotients (Q_r) of CO/CO_2 methanation and WGS reactions at outlet stream compositions.

drop for Ni/βCD-CeO_2 was caused by the much smaller size of the Ni nanoparticles on the surface of the CeO_2, which had an extremely high surface energy and specific surface area which are more prone to migration and sintering. Even though active support was chosen and high integration between the Ni and CeO_2 was detected (H_2-TPR tests), the Ni agglomerated in 24 h, even though the methane yield and selectivity maintained higher values for the Ni/βCD-CeO_2. A slight increase in CO2 generation caused no drop in CO conversion for the Ni/βCD-CeO_2.

To determine the extent of CO/CO_2 methanation and WGS reactions (WGSR), the temperature-dependent nonequilibrium reaction quotient Q_r values were calculated (Fig. 8.) concerning only a single reaction type for simplification. The trends also gave an overall view at the processes dynamics based on composition of the exhaust gas mixture. The WGSR operates near thermodynamic equilibrium point of reaction (Q_r~1) at elevated temperatures although it favours the formation of products at lower temperatures. This is due to the domination of fast reaction kinetics. The WGS at temperatures over 550 °C showed similar behaviour for all catalytic systems reaching nearly full thermodynamic equilibrium state. This corresponded well with decreasing CO_2 production rate (Figs. 5B and 6B) with increasing temperature. The WGS was more pronounced for Co/CeO_2 catalysts. The reaction rate of WGSR at intermediate temperatures was lower for Ni/CeO_2 catalyst. This trend was attributed to the decrease of WGS activity with an increase in the size of the Ni nanoparticles. Similar behaviour was observed for other WGS catalysts [78,79]. Ni-βCD/CeO_2 revealed outstanding activity towards performing both CO and CO_2 methanation compared to other catalysts as it was previously shown in Fig. 5. Both reactions are strongly shifting the composition of the outlet stream towards products with the most visible difference for Ni-βCD/CeO_2. The usage of cyclodextrin resulting in smaller and more active nanoparticles ensured stable performance of CO methanation from 550 °C onwards (Q_r plateau). The CO_2 methanation as a parallel reaction played a secondary role in the whole process using up the CO_2 created by WGSR. Clear contribution was visible in intermediate temperature region where also a decrease of CO_2 yield was observed (Fig. 5A). For both CH_4 generating reactions, the kinetics were poorer for Co containing samples. No significant difference was noticed in the quotient change trends between Co-βCD/CeO_2 and Co/CeO_2. Worth mentioning is the surprisingly stable and similar trend observed for both CO and CO_2 methanation in Co–CeO_2 systems. This would be crucial in real life SOEC chamber atmosphere containing a mixture of CO and CO_2, where cobalt could be even more suitable than nickel as an efficient catalyst [80,81].

The high working temperature of SOECs is the main problem when investigating new and efficient catalysts based on Ni. Future studies over catalysts for SOEC applications will concentrate on alloying two or more transition metals to achieve the synergistic effects of both components. As an example, the addition of Co into Ni nanoparticles should improve the high-temperature stability while maintaining the high activity of the Ni.

Conclusions

The purpose of this work was to synthesise and insightfully characterise the prepared catalysts based on nanometric CeO_2. The ceria support material was decorated with nanoparticles of transition metals via a simple wet-impregnation method. The addition of βCD resulted in the creation of smaller nanoparticles compared to the conventional method of impregnation. The size-reduction effect and increase in interfacial integration were highly pronounced especially for Ni, Co and Cu samples when cyclodextrin was used. The XRD and TPR studies gave an interesting description of the phase structure and reducibility. The additive produced strongly anchored metallic nanoparticles connected to the support by an interlayer of mixed ceria compound. The synergy between metal and CeO_2 increased the stability during cyclic reduction. The additional data proved the decomposition of mixed oxide phases under a reducing atmosphere. The catalyst-specific

Please cite this article as: Błaszczak P et al., Preparation of methanation catalysts for high temperature SOEC by β-cyclodextrin-assisted impregnation of nano-CeO_2 with transition metal oxides, International Journal of Hydrogen Energy, https://doi.org/10.1016/j.ijhydene.2021.10.144

surface was higher when βCD was added into the precursor solution. The catalytic activity towards methane synthesis was observed only for Ni- and Co-containing catalysts. The addition of βCD strongly influenced the final CO conversion and CH_4 selectivity parameters of the prepared catalysts. Ni-βCD/CeO_2 reached around 99% of CO conversion at 375 °C with nearly 80% selectivity to CH_4. The samples with a Co phase resulted in lower concentrations of CH_4 in the outlet stream, but again the positive influence of the βCD additive was observed. The stability of Ni nanoparticles in Ni-βCD/CeO_2 was a bit lower than in conventional samples due to the high surface energy of the created nanoparticles, which was not visible in the case of Co-βCD/CeO_2. The Co-βCD/CeO_2 sample peaked at 450 °C with around 84% CO conversion and nearly 60% CH_4 selectivity values. The presented studies proved that both the usage of transition metals with CeO_2 and the addition of small amounts of βCD could create a promising catalyst for SOEC applications. Further studies should be strongly concentrated on Ni–Co alloyed nanoparticles to give rise to the synergistic effects coming from both components.

Declaration of competing interest

The authors declare that they have no known competing financial interests or personal relationships that could have appeared to influence the work reported in this paper.

Acknowledgements

This work was supported by the 5th Polish-Taiwanese/Taiwanese-Polish Joint Research Project PL-TW/V/4/2018 granted by the National Centre for Research and Development of Poland and the Ministry of Science and Technology of Taiwan.

Appendix A. Supplementary data

Supplementary data to this article can be found online at https://doi.org/10.1016/j.ijhydene.2021.10.144.

REFERENCES

[1] Küngas R. Review—electrochemical CO2 reduction for CO production: comparison of low- and high-temperature electrolysis technologies. J Electrochem Soc 2020;167:44508. https://doi.org/10.1149/1945-7111/ab7099.
[2] Miao B, Ma SSK, Wang X, Su H, Chan SH. Catalysis mechanisms of CO2 and CO methanation. Catalysis Science & Technology 2016;6:4048–58. https://doi.org/10.1039/C6CY00478D.
[3] Wang H, Pei Y, Qiao M, Zong B. Advances in methanation catalysis. Catalysis 2017;29:1–28. https://doi.org/10.1039/9781788010634-00001. 2017.
[4] Anderson RB, Lee CB, Machiels JC. Can J Chem Eng 1976;54:590.
[5] Zheng Yun, Wang Jianchen, Yu Bo, Zhang Wenqiang, Chen Jing, Qiao Jinli, Zhang Jiujun. A review of high temperature co-electrolysis of H 2 O and CO 2 to produce sustainable fuels using solid oxide electrolysis cells (SOECs): advanced materials and technology. Chem Soc Rev 2017;46. https://doi.org/10.1039/C6CS00403B.
[6] Vannice M. Catal Rev: Sci Eng 1976;14:153.
[7] Li H, Ren J, Qin X, Qin Z, Lin J, Li Z. RSC Adv 2015;5:96504.
[8] Liu Q, Zhong Z, Gu F, Wang X, Lu X, Li H, Xu G, Su F. J Catal 2016;337:221.
[9] Li Z, Liu J, Wang H, Wang E, Wang B, Ma X, Qin S, Sun Q. J Mol Catal Chem 2013;378:99.
[10] Montini T, Melchionna M, Monai M, Fornasiero P. Fundamentals and catalytic applications of CeO2-based materials. Chem Rev 2016;116:5987–6041. https://doi.org/10.1021/acs.chemrev.5b00603.
[11] Wu T, Vegge T, Hansen HA. Improved electrocatalytic water splitting reaction on CeO2(111) by strain engineering: a DFT+U study. ACS Catal 2019;9:4853–61. https://doi.org/10.1021/acscatal.9b00203.
[12] Movasati A, Alavi SM, Mazloom G. Dry reforming of methane over CeO2-ZnAl2O4 supported Ni and Ni-Co nano-catalysts. Fuel 2019;236:1254–62. https://doi.org/10.1016/j.fuel.2018.09.069.
[13] Carrasco J, Barrio L, Liu P, Rodriguez JA, Ganduglia-Pirovano MV. J Phys Chem C 2013;117:824.
[14] Nematollahi B, Rezaei M, Lay EN. J Rare Earths 2015;33:619.
[15] Zeng Y, Ma H, Zhang H, Ying W, Fang D. Fuel 2015;162:16.
[16] Ma Z, Zhou J, Li Y, Liu C, Pu J, Chen X. Developments in CO2 electrolysis of solid oxide electrolysis cell with different cathodes. Fuel Cell 2020;20:650–60. https://doi.org/10.1002/fuce.201900240.
[17] Schaaf Tanja, Grünig Jochen, Schuster Markus, Rothenfluh Tobias, Orth Andreas. Methanation of CO2 - storage of renewable energy in a gas distribution system. Energy, Sustainability and Society 2014;4. https://doi.org/10.1186/s13705-014-0029-1.
[18] Atzori Luciano, Rombi E, Meloni D, Sini MF, Monaci R, Cutrufello MG. CO and CO2 Co-methanation on Ni/CeO2-ZrO2 soft-templated catalysts. Catalysts 2019;9(Issue 5). https://doi.org/10.3390/catal9050415.
[19] Nematollahi B, Rezaei M, Lay EN. Selective methanation of carbon monoxide in hydrogen rich stream over Ni/CeO2 nanocatalysts. J Rare Earths 2015;33:619–28. https://doi.org/10.1016/S1002-0721(14)60462-2.
[20] Italiano C, Llorca J, Pino L, Ferraro M, Antonucci V, Vita A. CO and CO2 methanation over Ni catalysts supported on CeO2, Al2O3 and Y2O3 oxides. Appl Catal B Environ 2020;264:118494. https://doi.org/10.1016/j.apcatb.2019.118494.
[21] Ai H, Liu Q, Yang H. W-doped ordered mesoporous Ni–Al2O3 catalyst for methanation of carbon monoxide. Int J Hydrogen Energy 2019;44:23975–82. https://doi.org/10.1016/j.ijhydene.2019.07.115.
[22] Hwang S, Lee J, Hong UG, Jung JC, Koh DJ, Lim H, Byun C, Song IK. Hydrogenation of carbon monoxide to methane over mesoporous nickel-M-alumina (M=Fe, Ni, Co, Ce, and La) xerogel catalysts. J Ind Eng Chem 2012;18:243–8. https://doi.org/10.1016/j.jiec.2011.11.026.
[23] Zhang Y, Zhang G, Wang L, Xu Y, Sun Y. Selective methanation of carbon monoxide over Ru-based catalysts in H2-rich gases. J Ind Eng Chem 2012;18:1590–7. https://doi.org/10.1016/j.jiec.2012.02.017.
[24] Najafpour Mohammad, Kaboudin Babak, Mostafalu Ramin, Shahbazy Mohammad, Safdari Rasoul, Kompany-Zareh, Mohsen. A proposed mechanism to form nanosized Mn oxides from the decomposition of β-cyclodextrin-Mn complex: toward nanosized water-splitting catalysts with special morphology. Int J Hydrogen Energy 2017;42. https://doi.org/10.1016/j.ijhydene.2017.03.005.

Please cite this article as: Błaszczak P et al., Preparation of methanation catalysts for high temperature SOEC by β-cyclodextrin-assisted impregnation of nano-CeO_2 with transition metal oxides, International Journal of Hydrogen Energy, https://doi.org/10.1016/j.ijhydene.2021.10.144

[25] Liu Huimin, Li Yuming, Wu Hao, Miyake Takanori, He Dehua. CO2 reforming of methane over Ni/SBA-15 prepared with β-cyclodextrin – role of β-cyclodextrin in Ni dispersion and performance. Int J Hydrogen Energy 2013;38:15200–9. https://doi.org/10.1016/j.ijhydene.2013.09.095.
[26] Noël S, Ponchel A, Sadjadi S, Monflier E, Léger B. Metal nanoparticles and cyclodextrins for catalytic applications. In: Crini G, Fourmentin S, Lichtfouse E, editors. The history of cyclodextrins. Environmental Chemistry for a sustainable world, vol. 52. Cham: Springer; 2020. https://doi.org/10.1007/978-3-030-49308-0_5.
[27] Hussain Ijaz. New insights on the effect of the H2/CO ratio for enhancement of CO methanation over metal-free fibrous silica ZSM-5: thermodynamic and mechanistic studies. Energy Convers Manag 2019;199:112056. https://doi.org/10.1016/j.enconman.2019.112056.
[28] Chlipała M, Błaszczak P, Wang S-F, Jasinski Piotr, Bochentyn Beata. In situ study of a composition of outlet gases from biogas fuelled Solid Oxide Fuel Cell performed by the Fourier Transform Infrared Spectroscopy. Int J Hydrogen Energy 2019;44. https://doi.org/10.1016/j.ijhydene.2019.03.243.
[29] Jean-Marie Alan, Griboval-Constant Anne, Khodakov Andrei, Monflier Eric, Diehl Fabrice. β-Cyclodextrin for design of alumina supported cobalt catalysts efficient in Fischer–Tropsch synthesis. Chem Commun 2011;47:10767–9. https://doi.org/10.1039/c1cc13800f.
[30] Liu Huimin, Li Yuming, Wu Hao, Jiaxiong Liu, He Dehua. Effects of α- and γ-cyclodextrin-modified impregnation method on physicochemical properties of Ni/SBA-15 and its catalytic performance in CO2 reforming of methane. Chin J Catal 2015;36. https://doi.org/10.1016/S1872-2067(14)60242-4.
[31] Odedairo Taiwo, Chen Jiuling, Zhu Zhonghua. Metal–support interface of a novel Ni–CeO2 catalyst for dry reforming of methane. Catal Commun 2013;31:25–31. https://doi.org/10.1016/j.catcom.2012.11.008.
[32] Giordano Francesca, Trovarelli Alessandro, Leitenburg Carla, Giona Massimiliano. A model for the temperature-programmed reduction of low and high surface area ceria. Journal of Catalysis - J CATAL. 2000;193:273–82. https://doi.org/10.1006/jcat.2000.2900.
[33] Cristhiane Guimarães Maciel, Tatiana de Freitas Silva, Marcelo Iuki Hirooka, Mohamed Naceur Belgacem, Jose Mansur Assaf. Effect of nature of ceria support in CuO/CeO2 catalyst for PROX-CO reaction. Fuel 2012;97:245–52. https://doi.org/10.1016/j.fuel.2012.02.004. ISSN 0016-2361.
[34] Gangavarapu Ranga Rao, Mishra Braja. Structural, redox and catalytic Chemistry of ceria based materials. Bull. Catal. Soc. India. 2003;2.
[35] Xu Jiahui, Harmer Jeffrey, Li Guoqiang, Chapman Thomas, Collier Paul, Longworth-Cook Sarennah, Tsang Shik. Size dependent oxygen buffering capacity of ceria nanocrystals. Chem Commun 2010;46:1887–9. https://doi.org/10.1039/b923780a.
[36] Zhou X-D, Huebner Wayne. Size-induced lattice relaxation in CeO2 nanoparticles. Appl Phys Lett 2001;79:3512–4. https://doi.org/10.1063/1.1419235.
[37] Xu Wenqian, Liu Zongyuan, Johnston-Peck Aaron, Senanayake Sanjaya, Zhou Gong, Stacchiola Dario, Stach Eric, Rodriguez José. Steam reforming of ethanol on Ni/CeO2: reaction pathway and interaction between Ni and the CeO2 support. ACS Catal 2013;3:975–84. https://doi.org/10.1021/cs4000969.
[38] Tang Changjin, Sun Bowen, Sun Jingfang, Hong Xi, Deng Yu, Gao Fei, Dong Lin. Solid state preparation of NiO-CeO2 catalyst for NO reduction. Catal Today 2016;281. https://doi.org/10.1016/j.cattod.2016.05.026.
[39] Shan Wenjuan, Luo Mengfei, Ying Pinliang, Shen Wenjie, Li Can. Reduction property and catalytic activity of Ce1–XNiXO2 mixed oxide catalysts for CH4 oxidation. Appl Catal Gen 2003;246:1–9. https://doi.org/10.1016/S0926-860X(02)00659-2.
[40] Pino Lidia, Vita Antonio, Cipitì Francesco, Laganà Massimo, Recupero Vincenzo. Catalytic performance of Ce1–xNixO2 catalysts for propane oxidative steam reforming. Catal Lett 2007;122:121–30. https://doi.org/10.1007/s10562-007-9357-5.
[41] Jehng Jih-Mirn, Chen Chia-Ming. Amination of polyethylene glycol to polyetheramine over the supported nickel catalysts. Catal Lett 2001;77:147–54. https://doi.org/10.1023/A:1012782927451.
[42] Zou Weixin, Ge Chengyan, Lu Minyue, Wu Shiguo, Wang Yongzheng, Sun Jingfang, Pu Yu, Tang Changjin, Gao Fei, Dong Lin. Engineering the NiO/CeO2 interface to enhance the catalytic performance for CO oxidation. RSC Adv 2015;5. https://doi.org/10.1039/C5RA20466F.
[43] Mierczynski Pawel, Mierczynska-Vasilev Agnieszka, Ciesielski Radoslaw, Mosińska Magdalena, Nowosielska Magdalena, Czylkowska A, Maniukiewicz Waldemar, Szynkowska Malgorzata, Vasilev Krasimir. High active and selective Ni/CeO2–Al2O3 and Pd–Ni/CeO2–Al2O3 catalysts for oxy-steam reforming of methanol. Catalysts 2018;8:380. https://doi.org/10.3390/catal8090380.
[44] Spadaro L, Arena Francesco, Granados M, Ojeda Monica, Fierro JLG, Frusteri Francesco. Metal–support interactions and reactivity of Co/CeO2 catalysts in the Fischer–Tropsch synthesis reaction. J Catal 2005;234:451–62. https://doi.org/10.1016/j.jcat.2005.07.006.
[45] Martınez-Arias A, Fernández-García Marcos, Gálvez Oscar, Coronado Juan, Anderson James, Conesa José C, Soria Javier, Munuera Guillermo. Comparative study on redox properties and catalytic behavior for CO oxidation of CuO/CeO 2 and CuO/ZrCeO 4 catalysts. Journal of Catalysis - J CATAL 2000;195:207–16. https://doi.org/10.1006/jcat.2000.2981.
[46] Luo Jin-Yong, Meng Ming, Li Xiang, Li Xingang, Zha Gangqiang, Hu Tiandou, Xie Ya-Ning, Zhang Jing. Mesoporous Co3O4–CeO2 and Pd/Co3O4–CeO2 catalysts: synthesis, characterization and mechanistic study of their catalytic properties for low-temperature CO oxidation. J Catal 2008;254:310–24. https://doi.org/10.1016/j.jcat.2008.01.007.
[47] Sohn Hyuntae, Celik Gokhan, Gunduz Seval, Dogu Doruk, Zhang Shiran, Shan Junjun, Tao Franklin, Ozkan Umit. Oxygen mobility in pre-reduced nano- and macro-ceria with Co loading: an AP-XPS, in-situ DRIFTS and TPR study. Catal Lett 2017;147:1–14. https://doi.org/10.1007/s10562-017-2176-4.
[48] Greluk Magdalena, Rotko Marek, Turczyniak-Surdacka, Sylwia. Enhanced catalytic performance of La2O3 promoted Co/CeO2 and Ni/CeO2 catalysts for effective hydrogen production by ethanol steam reforming. Renew Energy 2020;155. https://doi.org/10.1016/j.renene.2020.03.117.
[49] Nabaho Doreen, Niemantsverdriet Hans, Claeys M, Steen Eric. Hydrogen spillover in the Fischer–Tropsch synthesis: an analysis of platinum as a promoter for cobalt–alumina catalysts. Catal Today 2015;261. https://doi.org/10.1016/j.cattod.2015.08.050.
[50] Hołówko B, Błaszczak P, Chlipała M, Gazda Maria, Wang S-F, Jasinski Piotr, Bochentyn Beata. Structural and catalytic properties of ceria layers doped with transition metals for SOFCs fueled by biogas. Int J Hydrogen Energy 2020;45. https://doi.org/10.1016/j.ijhydene.2020.02.144.
[51] Yan Xingbin, Wang Xiaolai. Catalytic performances of NiO–CeO 2 for the reforming of methane with CO 2 and O 2. Fuel 2006;85:2243–7. https://doi.org/10.1016/j.fuel.2006.03.022.

Please cite this article as: Błaszczak P et al., Preparation of methanation catalysts for high temperature SOEC by β-cyclodextrin-assisted impregnation of nano-CeO_2 with transition metal oxides, International Journal of Hydrogen Energy, https://doi.org/10.1016/j.ijhydene.2021.10.144

[52] Ansari Anees, Labis Joselito, Alam Manawwer, Ramay Shahid, Ahmad Naushad, Mahmood Asif. Effect of cobalt doping on structural, optical and redox properties cerium oxide nanoparticles. Phase Transitions 2015;89:1–12. https://doi.org/10.1080/01411594.2015.1116532.
[53] Martınez-Arias A, Fernández-Garcıa M, Soria J, Conesa JC. Spectroscopic study of a Cu/CeO2Catalyst subjected to redox treatments in carbon monoxide and oxygen. J Catal 1999;182:367–77. https://doi.org/10.1006/jcat.1998.2361.
[54] Du Lin-Ying, Wang Wei-Wei, Yan Han, Wang Xu, Jin Zhao, Song Qi-Sheng, Si Rui, Jia Chun-Jiang. Copper-ceria sheets catalysts: effect of copper species on catalytic activity in CO oxidation reaction. J Rare Earths 2017;35. https://doi.org/10.1016/j.jre.2017.04.005.
[55] Luo M-F, Song Y-P, Lu Jiqing, Wang X-Y, Pu Z-Y. Identification of CuO species in high surface area CuO-CeO2 catalysts and their catalytic activities for CO oxidation. Journal of Physical Chemistry C - J PHYS CHEM C 2007;111:12686–92. https://doi.org/10.1021/jp0733217.
[56] Ren Zhibo, Peng Fei, Li Jianwei, Liang Xin, Chen Biaohua. Morphology-dependent properties of Cu/CeO2 catalysts for the water-gas shift reaction. Catalysts 2017;7:48. https://doi.org/10.3390/catal7020048.
[57] Zhan Sihui, Zhu Dandan, Qiu Mingying, Yu Hongbing, Li Yi. Highly efficient removal of NO with ordered mesoporous manganese oxide at low temperature. RSC Adv 2015;5:29353–61. https://doi.org/10.1039/C4RA17300G.
[58] Zhang Jianghao, Zhang Changbin, Yaobin Li, Wang Lian, He Hong. Catalytic oxidation of formaldehyde over manganese oxides with different crystal structures. Catal. Sci. Technol. 2015;5. https://doi.org/10.1039/C4CY01461H.
[59] Qu Zhenping, Fan Rui, Wang Zhong, Wang Hui, Miao Lei. Selective catalytic oxidation of ammonia to nitrogen over MnO2 prepared by urea-assisted hydrothermal method. Appl Surf Sci 2015;351. https://doi.org/10.1016/j.apsusc.2015.05.154.
[60] Fakeeha Anis, Barama Siham, Ibrahim Ahmed, Al-Otaibi, Raja-Lafi, Barama Akila, Abasaeed A, Alfatesh Ahmed. In situ regeneration of alumina-supported cobalt–iron catalysts for hydrogen production by catalytic methane decomposition. Catalysts 2018;8:567. https://doi.org/10.3390/catal8110567.
[61] Portnyagin As, Golikov A, Drozd Vladimir, Avramenko Valentin. An alternative approach to kinetic analysis of temperature-programmed reaction data. RSC Adv 2018;8:3286–95. https://doi.org/10.1039/C7RA09848K.
[62] Tiernan MJ, Barnes PA, Parkes GMB. Reduction of iron oxide catalysts: the investigation of kinetic parameters using rate perturbation and linear heating thermoanalytical techniques. J Phys Chem B 2001;105:220–8. https://doi.org/10.1021/jp003189.
[63] Prochowicz D, Kornowicz A, Lewiński J. Interactions of native cyclodextrins with metal ions and inorganic nanoparticles: fertile landscape for Chemistry and materials science. Chem Rev 2017;117:13461–501. https://doi.org/10.1021/acs.chemrev.7b00231.
[64] Jean-Marie Alan, Griboval-Constant Anne, Khodakov Andrei, Monflier Eric, Diehl Fabrice. β-Cyclodextrin for design of alumina supported cobalt catalysts efficient in Fischer–Tropsch synthesis. Chem Commun 2011;47:10767–9. https://doi.org/10.1039/c1cc13800f.
[65] Liu Huimin, Li Yuming, Wu Hao, Jiaxiong Liu, He Dehua. Effects of α- and γ-cyclodextrin-modified impregnation method on physicochemical properties of Ni/SBA-15 and its catalytic performance in CO2 reforming of methane. Chin J Catal 2015;36. https://doi.org/10.1016/S1872-2067(14)60242-4.
[66] Brunauer S, Deming LS, Deming WE, et al. On a theory of the van der Waals adsorption of gases. J Am Chem Soc 1940;62:1723–32.
[67] Yang Shuang, Chen Guojun, Lv Chengfu, Li Chao, Yin Na, Yang Fei, Xue Lianhua. Evolution of nanopore structure in lacustrine organic-rich shales during thermal maturation from hydrous pyrolysis, Minhe Basin, Northwest China, vol. 36. Energy Exploration & Exploitation; 2017. https://doi.org/10.1177/0144598717723647.
[68] Bharathi Niruban, Sankar S. Investigation of transport properties of Pr doped cerium oxide nanoparticles as a solid electrolyte for IT-SOFC applications. J Inorg Organomet Polym Mater 2018;28. https://doi.org/10.1007/s10904-018-0880-1.
[69] Liu Bai, Liu L, Liu X, Liu M, Xiao Y. Variation of crystal structure in nickel nanoparticles filled in carbon nanotubes. Mater Sci Technol 2009;28:1345–8. https://doi.org/10.1179/026708309X12526555493198.
[70] Ponnar M, Pushpanathan K, Santhi R, Ravichandran S. Enhanced supercapacitor performance and ferromagnetic behavior of Ni-doped CeO2 quantum dots. J Mater Sci Mater Electron 2020;31. https://doi.org/10.1007/s10854-020-03816-7.
[71] Shen L, Xu J, Zhu M, Han YF. Essential role of the support for nickel-based CO2 methanation catalysts. ACS Catal 2020;10:14581–91. https://doi.org/10.1021/acscatal.0c03471.
[72] Rossi Laura, Kinen Claudio, de Rossi Rita. Important role of native β -cyclodextrin in the stabilization of transition metal salts. Compt Rendus Chem 2017;20. https://doi.org/10.1016/j.crci.2017.09.007.
[73] Ciesielski Wojciech, Girek Tomasz. Study of thermal stability of β-cyclodextrin/metal complexes in the aspect of their future applications. J Inclusion Phenom 2011;69:461–7. https://doi.org/10.1007/s10847-010-9803-7.
[74] Tada Shohei, Shimizu Teruyuki, Kameyama Hiromichi, Haneda Takahide, Kikuchi Ryuji. Ni/CeO2 catalysts with high CO2 methanation activity and high CH4 selectivity at low temperatures. Int J Hydrogen Energy 2012;37:5527–31. https://doi.org/10.1016/j.ijhydene.2011.12.122.
[75] Tu J, Wu H, Qian Q, Han S, Chu M, Jia S, et al. Low temperature methanation of CO2 over an amorphous cobalt-based catalyst. Chem Sci 2021;12:3937–43. https://doi.org/10.1039/d0sc06414a.
[76] Xu Y, Wu Y, Li J, Wei S, Gao X, Wang P. Combustion-impregnation preparation of Ni/SiO2 catalyst with improved low-temperature activity for CO2 methanation. Int J Hydrogen Energy 2021;46:20919–29. https://doi.org/10.1016/j.ijhydene.2021.03.201.
[77] Tada S, Nagase H, Fujiwara N, Kikuchi R. What are the best active sites for CO2 methanation over Ni/CeO2? Energy Fuel 2021;35:5241–51. https://doi.org/10.1021/acs.energyfuels.0c04238.
[78] Senanayake Sanjaya, Evans Jaime, Agnoli Stefano, Barrio Laura, Chen Tsung-Liang, Hrbek Jan, Rodriguez José. Water–gas shift and CO methanation reactions over Ni–CeO 2 (111) catalysts. Top Catal 2011;54:34–41. https://doi.org/10.1007/s11244-011-9645-6.
[79] Rodriguez Jg, Liu P, Wang X, Wen Wen, Hanson Jonathan, Hrbek Jan, Perez Marilena, Evans J. Water-gas shift activity of Cu surfaces and Cu nanoparticles supported on metal oxides. Catal Today 2009;143:45–50. https://doi.org/10.1016/j.cattod.2008.08.022.
[80] Liang Chuanfei, Tian Hongli, Gao Guoming, Zhang Shu, Liu Qing, Dong Dehua, Hu Xun. Methanation of CO2 over alumina supported nickel or cobalt catalysts: effects of the coordination between metal and support on formation of the reaction intermediates. Int J Hydrogen Energy 2019;45. https://doi.org/10.1016/j.ijhydene.2019.10.195.
[81] Díez Javier, Sánchez Paula, Kyriakou Vasileios, Zafeiratos S, Marnellos George, Konsolakis Michalis, Dorado Fernando. Effect of support nature on the cobalt-catalyzed CO 2 hydrogenation. Journal of CO2 Utilization 2017;21:562–71. https://doi.org/10.1016/j.jcou.2017.08.019.

Please cite this article as: Błaszczak P et al., Preparation of methanation catalysts for high temperature SOEC by β-cyclodextrin-assisted impregnation of nano-CeO_2 with transition metal oxides, International Journal of Hydrogen Energy, https://doi.org/10.1016/j.ijhydene.2021.10.144